Molecular dynamics study of an isomerizing diatomic in a Lennard-Jones fluid[a)]

John E. Straub,[b)] Michal Borkovec,[c)] and Bruce J. Berne
Department of Chemistry, Columbia University, New York, New York 10027

(Received 17 February 1988; accepted 20 May 1988)

The behavior of the reaction rate of an isomerizing diatomic molecule solvated in a Lennard-Jones fluid is studied by molecular dynamics simulations. A comprehensive study of solvation effects on the rate constant, using the reactive flux absorbing boundary approximation of Straub and Berne, is presented. We provide simulation data over three orders of magnitude in solvent density for four systems differing in the mass of the solvent atoms and frequencies of the internal potential. Rate constants are also calculated for the model system using both Langevin Dynamics with exponential memory and impulsive collision dynamics of the BGK model. A simple method for calculating the average energy transfer and collision frequency is used to determine the collision efficiency for systems in which the mass of the solvent atoms is lighter than, equal to, or heavier than that of the atoms composing the isomerizing diatomic. We find that for solvents of equal and heavy mass compared to the solute the impulsive collision model provides the best description of the dynamics. Finally, we employ a method recently introduced by us to calculate the spatial dependence of the dynamic friction; we compare the reaction coordinate friction at the transition state separation with an approximation based on the single particle friction. This directly calculated reaction coordinate friction, when combined with the Grote–Hynes theory for barrier crossing, gives good agreement with the simulation data at high density.

I. INTRODUCTION

Transition state theory provided the first theoretical predictions of absolute reaction rates for chemical reactions.[1] As expressed by Eyring[2] and Wigner,[3] the rate constant is the probability of having the activation energy, multiplied by the equilibrium "reaction velocity" for crossing the transition state surface separating reactants and products. Additionally, a prefactor, the transmission coefficient, is included to account for the possibility of crossing the transition state to the product region and then recrossing to the reactant state before deactivation.

In recent years renewed interest in these questions has been stimulated by novel theoretical ideas[4–6] and new experimental techniques. The experiments have provided chemical reaction rate constant data as a function of the pressure or viscosity of the solvent.[7–11] Much of this work has been stimulated by interest in Kramers theory and its recent extensions.[12–14] These theories concentrate on the deviations from transition state theory or the calculation of the transmission coefficient—quantifying recrossings of the transition state.

There is a whole cascade of approximations made in interpreting the experimentally observed rate constant of a reacting molecule in a solvent in terms of theoretical models. First of all, one has to invoke the Born–Oppenheimer approximation to separate the electronic and nuclear degrees of freedom. Then, when the ground state potential surface is given, one often approximates the motion of the nuclei by classical mechanics. The potential surface arises from the potential surfaces of the reacting molecule (solute), solvent–solute interactions, and solvent–solvent interactions. A potential surface can be determined by *ab initio* calculation[15] or using semiempirical force fields. The details of the surface, such as the activation energy separating reactant and product states and the frequencies of the well and barrier regions, are usually derived from spectroscopic data[10] or fits to theoretical predictions after assuming a simple potential form.[7] Femtosecond lasers should soon provide much greater certainty and detail.[16] Nevertheless, the determination of a sufficiently accurate potential surface is very often not feasible and this point provides the major stumbling block for the application of the powerful molecular dynamics methods to problems of chemical interest. The interaction between the reacting molecule and the solvent molecules is often not known. It must then suffice to model this interaction by approximate semiempirical force fields.

Once the potential surface of the many-body system is determined, the chemical rate constant can be evaluated on a computer by brute force application of modern algorithms. Nevertheless, such an approach does not help in the understanding of the physical processes determining the rate constant. To gain such an understanding further abstraction from the real system is necessary. For example, when the solvent moves rapidly compared to the solute, a substantial simplification can be introduced by approximating the action of the solvent by a modified potential surface for the solute, the potential of mean force, and a stochastic bath which captures the main dynamic features of the solvent.

The choice of those degrees of freedom considered to be the "bath" and those belonging to the "system" is a matter of convenience. The simplest choice for the system is one particular reaction coordinate; the bath is composed of all remaining degrees of freedom. An intuitively appealing choice is to view the whole reacting molecule as the system and the solvent degrees of freedom as the bath.

[a)] Supported by a grant from the NSF.
[b)] Present address: Department of Chemistry, Harvard University, Cambridge, Massachusetts 02138.
[c)] Present address: Institut für Physikalische Chemie, Universität Basel, Klingelbergstr 80, 4056 Basel, Switzerland.

 0021-9606/88/204833-15$02.10

The bath can be modeled on different levels of complexity. The classical Kramers model[17] is probably the simplest, i.e., a Langevin constant friction model or the impulsive collisional BGK model.[18] Better description is possible by more refined collisional models[11] or by incorporating the finite response time of the solvent using a frequency dependent friction.[12] The friction coefficient can be modeled in a variety of ways. It can be thought of as friction acting on different sites in the molecule. In such cases, mode coupling theories and molecular hydrodynamics have been capable of producing models of the friction coefficient for some simple systems.[19,20] Fortunately, computer simulation techniques have recently been developed which are capable of extracting this information on arbitrarily complicated systems.[21]

Finally, once the stochastic bath has been chosen, the rate constant for such a system must be evaluated. In many cases this is possible analytically.[13,22] Rate coefficients describing the *activation process* increase strongly with the exact number of degrees of freedom that equipartition energy with the reaction coordinate on the time scale of the reaction. Because the time scale of the reaction decreases with the collision frequency or the friction coefficient, the effective number of degrees of freedom should decrease and the rate constant should increase more and more slowly as the collision frequency or friction coefficient is increased.[23–26] This is in the spirit of unimolecular rate theory[11,26] The *barrier crossing* step is less sensitive to the exact number of degrees of freedom coupled to the reaction coordinate, but depends strongly on the details of the friction or collision frequency affecting the reaction coordinate.[27–29] Such an approach can be viewed as generalized transition state theory.[30]

Given a stochastic model for the bath the problem of calculating the rate constant has received substantial attention recently. Examples where analytical evaluation is possible are, e.g., the Kramers or BGK model for a single[4,5] or several[25,31] strongly coupled degrees of freedom, and non-Markovian models[6] for not too large correlation times. On the other hand, one has to face the fact that there are systems where no analytical theories for evaluation of the rate constant are available.[32] In such cases, applications of existing analytical theories yield incorrect rate constants. This point is particularly subtle as only few criteria are known at present to judge the validity of analytical theories.[13,24,29,32] A typical example is the caging effect for an exponential friction kernel at large correlation times which reduces drastically the rate constant—an approximate bridging formula can overestimate the rate constant by orders of magnitude.[32] In other studies, the efficiency of vibrational energy transfer and the rate of collision between the solvent and the reaction coordinate have been studied to determine the validity of strong collision models.[24,29,33] There it was found that detailed knowledge of the density of vibrational states which can equipartition energy with the reaction coordinate on the time scale of the reaction was prerequisite for an accurate application of the theories.

It is quite obvious that a simple choice of the bath results in an oversimplification of the real action of the solvent on the reacting molecule but allows a simple calculation of the rate constants and vice versa. For example, a one degree of freedom Kramers model, which might be a poor model for the action of the solvent on the reaction coordinate, requires only the evaluation of a single parameter (friction coefficient) and it is an easy matter to calculate the rate constant from potential parameters. On the other hand, a model with several degrees of freedom coupled to a non-Markovian bath, which might be an excellent model for the bath, requires the nontrivial evaluation of frequency dependent friction kernels and often makes the analytical evaluation of corresponding rate constants subject to large uncertainties.

Rate constants are measured experimentally as a function of solvent density, viscosity, or pressure. In order to compare these findings with theoretical models a large number of assumptions and simplifications are introduced. For example, the system is treated classically, the friction on the reaction coordinate is approximated by the friction on a sphere in a viscoelastic continuum solvent, or the effects of the potential of mean force are neglected. Obviously, such an array of approximations is essentially impossible to control in a realistic system, where many parameters are not well known in advance. For this reason, a molecular dynamics study of a system, in which one can control the parameters, can be of great value in providing insights. This cannot be done experimentally.

In this paper we make use of recent developments in numerical techniques and present the results of such a study. Our first priority was to choose a system where all relevant quantities can be calculated with sufficient accuracy. This imposes severe restrictions on the system. Actually, we have to confess that the present lack of knowledge of potential surfaces, solvent models, and interactions between reactant and fluid makes it difficult to simulate real experimental systems. Therefore, we study an idealized system—the isomerization rate of a model diatomic molecule in a Lennard-Jones fluid. The bond length can jump continuously between two bound metastable states separated by an activation barrier. In Sec. II we describe the equilibrium and time dependent properties of a Lennard-Jones fluid. Section III details the reaction system, summarizes the theoretical models used to interpret our simulation data, and discusses our simulation of the rate constants for four systems of different internal potential or solvent mass. In Sec. IV we discuss in detail the input for the various theoretical predictions in the form of the collision efficiency and reaction coordinate friction, and we present stochastic simulation data for our system which addresses the accuracy of the theories in going from the assumed equations of motion to the rate constant. Section V discusses the relevance of this study for the interpretation of other reaction systems.

II. PROPERTIES OF A LENNARD-JONES SOLVENT

In this section, we summarize the equilibrium structural and dynamic properties of neat Lennard-Jones fluid. The intermolecular potential for a system of atoms of type A is

$$U_{AA}(r) = 4\epsilon_{AA}\left[\left(\frac{\sigma_{AA}}{r}\right)^{12} - \left(\frac{\sigma_{AA}}{r}\right)^{6}\right], \tag{2.1}$$

where the Lennard-Jones reduced units are used in which

the atomic mass m_A, radius σ_{AA}, well depth ϵ_{AA}, and Boltzmann's constant k_B are equal to unity. $(m_A\sigma_{AA}^2/\epsilon_{AA})^{1/2}$ is the unit of time and the reduced density $\rho = n_A\sigma_{AA}^3$. All our data is for the reduced temperature $\hat{T} = k_BT/\epsilon_{AA} = 2.5$.

Calculations were performed using a fifth order Gear predictor–corrector algorithm[34] on an FPS-164 attached processor.[35] This algorithm naturally generates higher order time derivatives of the velocity which are useful in the calculation of time correlation functions. The time step was 2×10^{-3}.

A. Equilibrium properties

The potential of mean force between two particles is defined by[36,37]

$$w(r) = -k_BT\ln g(r) \tag{2.2}$$

in terms of the radial distribution function $g(r)$.[36] This can be expressed as $w(r) = U(r) + \Delta W(r)$ where $U(r)$ is the bare two body potential, and $\Delta W(r)$ is the solvent induced part of the potential of mean force.

In Fig. 1 the potential of mean force is displayed for a Lennard-Jones fluid at a reduced temperature $\hat{T} = 2.5$ for several densities. These results are well reproduced by the function

$$\Delta W(r) = \frac{a_1r^2}{a_2^2 + r^6}\cos(\alpha r - \beta) + \frac{a_3 + a_4r^2}{a_5^2 + r^8} \tag{2.3}$$

which is accurate for $r > 0.7$. The necessary coefficients are listed in Table I.

TABLE I. Coefficients for Eq. (2.3).

ρ	a_1	a_2	a_3	a_4	a_5	α	β
<0.50	-9.7ρ	3.05	-0.73ρ	0.14ρ	0.48	2.7	1.4
0.50	−2.8	2.84	−9.6	7.9	1.56	5.7	0.15
0.70	−6.1	4.3	−16.0	12.3	1.52	6.4	0.82
0.80	−7.9	4.4	−17.1	13.3	1.37	6.5	0.68
0.95	−12.1	4.9	−21.7	16.7	1.36	6.6	0.29
1.05	−14.1	4.5	−21.5	17.4	1.10	6.9	0.66

B. Dynamic properties

In the theory of liquids, the generalized Langevin equation

$$m\ddot{x} = -\int_0^t dt'\,\zeta(t')\dot{x}(t-t') + R(t) \tag{2.4}$$

has played an important role in the definition and analysis of time dependent properties.[38,39] x is a coordinate describing the center of mass motion of a molecule, m is its mass, $\zeta(t)$ is the dynamic friction, and $R(t)$ the random force.[39,40] The dynamic friction $\zeta(t)$ specifies how the fluctuations in the velocity $\dot{x}$ will decay in time. It is defined by[41]

$$\dot{C}(t) = -\int_0^t dt'\,\frac{\zeta(t')}{m}\,C(t-t'), \tag{2.5}$$

where $C(t) = \langle\dot{x}(t)\dot{x}(0)\rangle/\langle\dot{x}^2\rangle$ is the velocity correlation function, and $\langle\cdots\rangle$ represents an equilibrium average over the canonical distribution function $e^{-\beta H}$ where H is the system Hamiltonian and $\beta = 1/k_BT$. $\zeta(t)$ can be calculated by numerically inverting this equation.[41]

In Fig. 2 the dynamic friction kernel $\zeta(t)$ is displayed as a function of time for several reduced densities. These results are accurately reproduced by the function

$$\zeta(t) = \zeta(0)[e^{-\alpha t^2}(1 + a_1t^4) + a_2t^4e^{-\beta t^2} + a_3t^6e^{-\gamma t^2}] \tag{2.6}$$

with coefficients $a_1 \approx 5.86\times10^4 + 9.0\times10^4\rho$, $a_2 \approx -385 + 670\rho^5$, $\alpha \approx 787 + 116\rho^2$, $\beta \approx 75.0$, and $\gamma \approx 1.0$. a_3 is adjusted from $\hat{\zeta}(0)$.[42] The latter quantity has been determined by the more accurate calculation of the diffusion coefficient D of the particles from the mean square displacement using the Einstein relation $\hat{\zeta}(0) = k_BT/D$. Figure 3 shows the

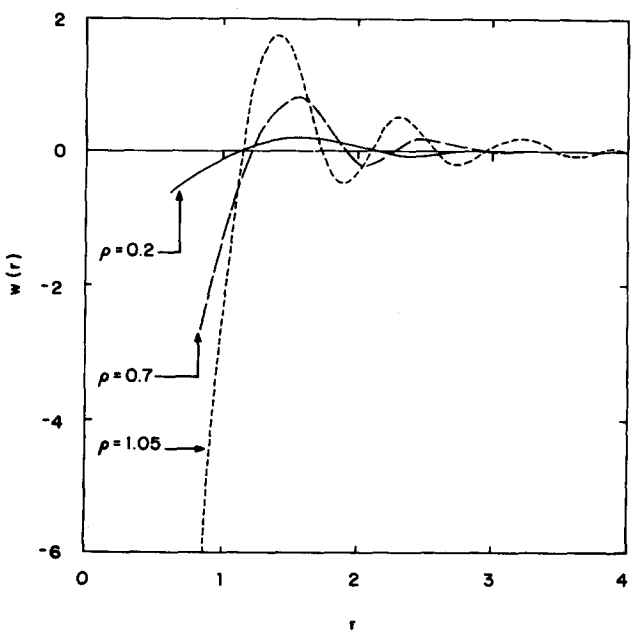

FIG. 1. The solvent contribution to the potential of mean force for a Lennard-Jones fluid. This simulation data is well fit by Eq. (2.3).

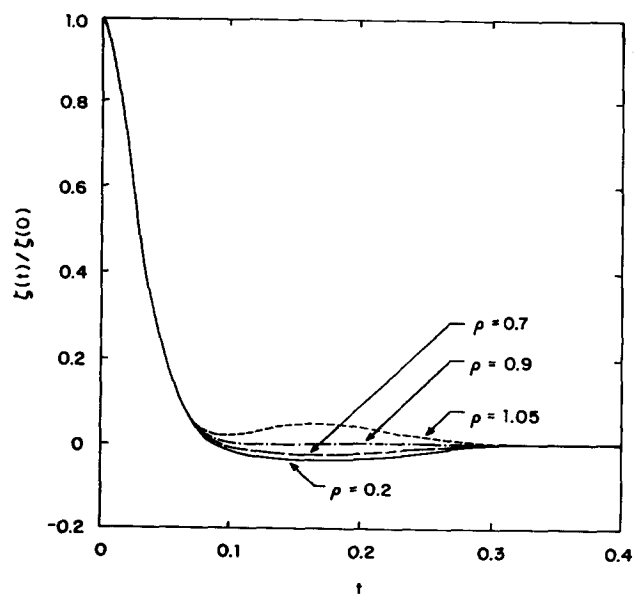

FIG. 2. The time dependent friction for a single atom of a Lennard-Jones fluid at several reduced densities. This simulation data is well fit by Eq. (2.6).

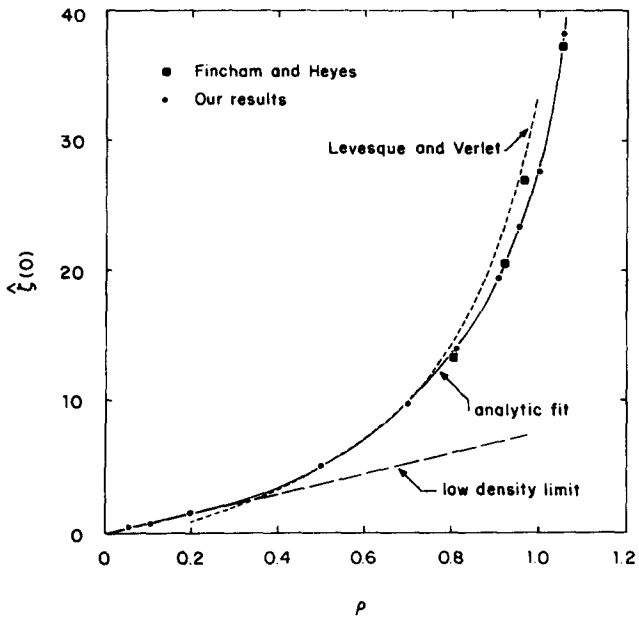

FIG. 3. The zero frequency, or time integrated value $\hat{\zeta}(0)$ of the dynamic friction $\zeta(t)$ for a Lennard-Jones fluid as a function of density. The fit to the data points is given by Eq. (2.7).

zero frequency friction coefficient as a function of density and is accurately fit by

$$\hat{\zeta}(0) \approx 7.47\rho + 7.19\rho^2 e^{1.1\rho^4}. \tag{2.7}$$

It can be seen that this fit to our data is in good agreement with the molecular dynamics data of Fincham and Heyes,[43] the approximate formula of Levesque and Verlet[44] valid for higher densities, as well as the analytic low density expansion.

The initial value of the friction kernel $\zeta(0)$ is the mean square force on the coordinate divided by the mean square momentum. It is independent of the mass of the solvent atoms forming the bath but will depend on the density.[36]

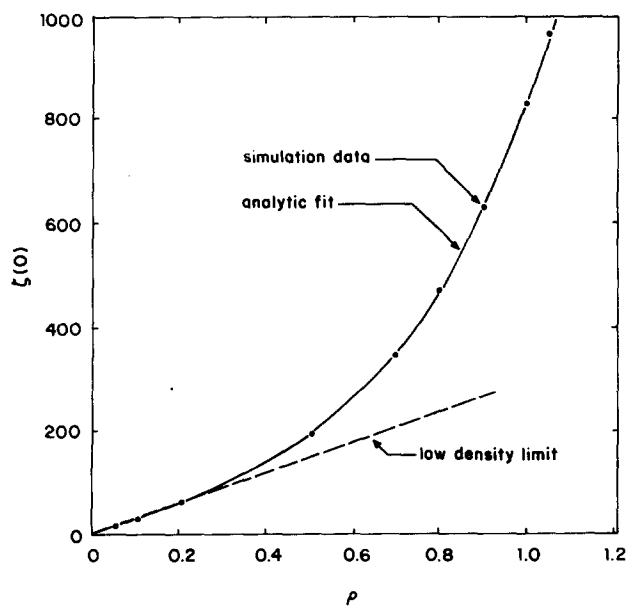

FIG. 4. The zero time value of the dynamic friction $\zeta(t)$ for a Lennard-Jones fluid as a function of density. The fit to the data points is given by Eq. (2.8).

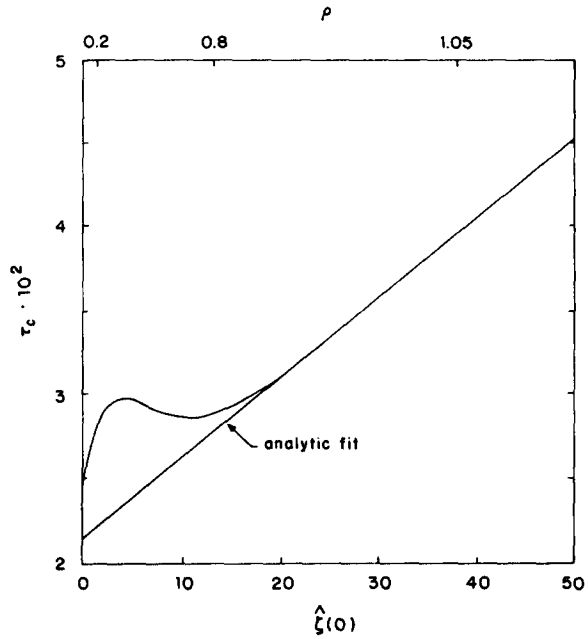

FIG. 5. The correlation time of the Lennard-Jones fluid as a function of the zero frequency friction for several densities. The solid line is the approximation of Eq. (2.9).

Figure 4 shows the initial value of the friction kernel as a function of density. The fit to the simulation points including the correct low density behavior is given by

$$\zeta(0) \approx 297\rho e^{1.02\rho^2}. \tag{2.8}$$

The correlation time of the liquid, defined here as $\tau_c = \hat{\zeta}(0)/\zeta(0)$ as with an exponential form, is shown in Fig. 5 for $\zeta(t)$, as a function of the zero frequency friction. It is worth noting that the simple linear relation between the correlation time and the zero frequency friction $\hat{\zeta}(0)$ greater than 20,

$$\tau_c \approx 0.0216 + 4.74 \times 10^{-4}\,\hat{\zeta}(0). \tag{2.9}$$

Such relations have been proposed previously.[19] Thus, at high friction (viscosity), τ_c increases linearly with the static friction coefficient $\hat{\zeta}(0)$.

To understand the dynamic friction, it is useful to think in terms of the Laplace transform, or frequency dependence, of the friction kernel

$$\hat{\zeta}(s) = \int_0^\infty dt\, e^{-st}\zeta(t), \tag{2.10}$$

where the value at a particular frequency s represents the dissipation experienced by a particle moving at that frequency. The static limit of the friction, i.e., the zero frequency friction, is the time integral of the dynamic friction kernel

$$\hat{\zeta}(0) = \int_0^\infty dt'\,\zeta(t'). \tag{2.11}$$

The dependence of the dynamic friction on the particular frequency of motion can be understood in terms of the cosine transform $Re\,\hat{\zeta}(-i\omega)$. This function, normalized by the zero frequency friction, is compared for a number of densities in Fig. 6. The maximum in the function is the frequency of motion most strongly damped by the surrounding solvent atoms.

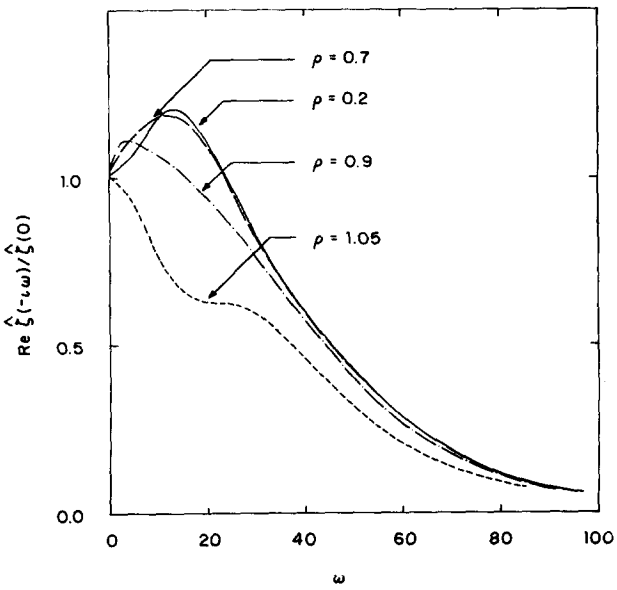

FIG. 6. The frequency dependence of the dynamic friction $\zeta(t)$ for a Lennard-Jones fluid for several densities.

III. CALCULATION OF RATE CONSTANTS

A. Reaction system

Our reaction system consists of a diatomic molecule A_2^* solvated in a fluid of atoms of type A. The solvent–solvent interaction is the standard Lennard-Jones type defined in Eq. (2.1). For simplicity the solute–solvent interaction is taken to be a two site LJ potential in which each A* interacts with each solvent atom through precisely the same potential,

$$U_{AA^*}(r) = 4\epsilon_{AA}\left[\left(\frac{\sigma_{AA}}{r}\right)^{12} - \left(\frac{\sigma_{AA}}{r}\right)^{6}\right]. \tag{3.1}$$

The diatomic intramolecular potential

$$\begin{aligned} U_{A^*A^*}(r) &= Q(1-\lambda^2 y^2) \quad \text{for} |y| < y_1 \\ &= Q(y-y_0)^2 \quad \text{for} |y| > y_1 \end{aligned} \tag{3.2}$$

is a symmetric bistable piecewise continuous potential with parabolic barrier and harmonic wells. y is defined by $r = a + (4Q/\omega_0^2)^{1/2} y$ where a is the position of the barrier maximum, Q is the barrier height, ω_B and ω_0 are the harmonic barrier and well frequencies, respectively, and $\lambda = \omega_B/\omega_0$ is their ratio. The well and barrier regions are joined continuously at y_1 and the well minima are located at $y = \pm y_0$, where $y_1^2\lambda^2(1+\lambda^2) = 1$ and $y_0 = y_1(1+\lambda^2)$. For the work discussed in this paper we use a value of $a = 1.25$.

The reaction itself is defined as follows. The diatomic molecule has a bistable internal potential providing two metastable states. Vibrations about the inner state constitute reactant while vibrations about the outer state constitute product. The reaction consists of transitions between these two states. The position of the barrier in the potential of mean force precisely defines the transitions from reactant to product.

B. Transitions state theory

The isomerization reaction

$$A \underset{k^b}{\overset{k^f}{\rightleftarrows}} B$$

has a total kinetic reaction rate constant $k = k^f + k^b$, the sum of the forward and backward rate constants. In general, the equilibrium rate constant can be conveniently written as[1,45]

$$k = \kappa k_{TST}, \tag{3.3}$$

where k is the true kinetic rate constant, k_{TST} is the transition state kinetic rate constant, and κ is the dynamic transmission coefficient measuring the deviation from transition state theory. When the forward (backward) transition state rate constant is inserted in Eq. (3.3) in place of k_{TST}, k is the forward (backward) rate constant. The transition state theory rate is the maximum possible rate constant so that κ is always less than or equal to unity.[46] The transmission coefficient is the same for the forward and backward reactions. Note that whereas k_{TST} and κ depend on the choice of reaction coordinate x, their product, i.e., the overall rate constant k, is independent of this choice.

The forward and backward transition state rate constants are given by[45]

$$k^f_{TST} = k^{in\to out}_{TST} = \frac{\langle \delta(q)\dot{q}\theta(\dot{q})\rangle}{\langle \theta(-q)\rangle}, \tag{3.4}$$

$$k^b_{TST} = k^{out\to in}_{TST} = \frac{\langle \delta(q)\dot{q}\theta(\dot{q})\rangle}{1-\langle \theta(-q)\rangle}, \tag{3.5}$$

where $q = r - a$ is the reaction coordinate, $\delta(q)$ defines the transition state, $\dot{q}$ is the reaction coordinate velocity, $\langle\cdots\rangle$ is a canonical average, and $\langle\theta(-q)\rangle$ is the unit step function that is unity in the reactant state (A). If the barrier height $Q \gg k_B T$, and the wells can be well approximated by harmonic oscillators, a good and convenient approximation for the one-dimensional reaction coordinate in the TST approximation for a symmetric double well is[46]

$$k^{1D}_{TST} \approx \frac{\omega_0}{2\pi} e^{-\beta Q}. \tag{3.6}$$

The absolute value of the rate constant k is the experimentally observed quantity. As we are also interested in deviations from the transition state theory predictions, the value of the transmission coefficient κ is of interest. It is important to understand the effects of solvation on the transition state theory rate where the equilibrium constant and activation energy is affected by the presence of solvent.

Detailed balance relates the ratio of the forward and backward rates to the equilibrium constant K_{eq}. If X_{in} and X_{out} are the equilibrium mole fractions for the inner and outer wells of the diatomic,

$$K_{eq} = \frac{k^{in\to out}}{k^{out\to in}} = \frac{X_{out}}{X_{in}} = \frac{\int_a^\infty e^{-\beta w(r)} r^2\, dr}{\int_0^a e^{-\beta w(r)} r^2\, dr}, \tag{3.7}$$

where $r = a$ is the position of the transition state and $w(r)$ is the potential of mean force. The r^2 terms in Eq. (3.7) can be added to the potential of mean force defined by Eq. (2.2), giving the effective potential of mean force,

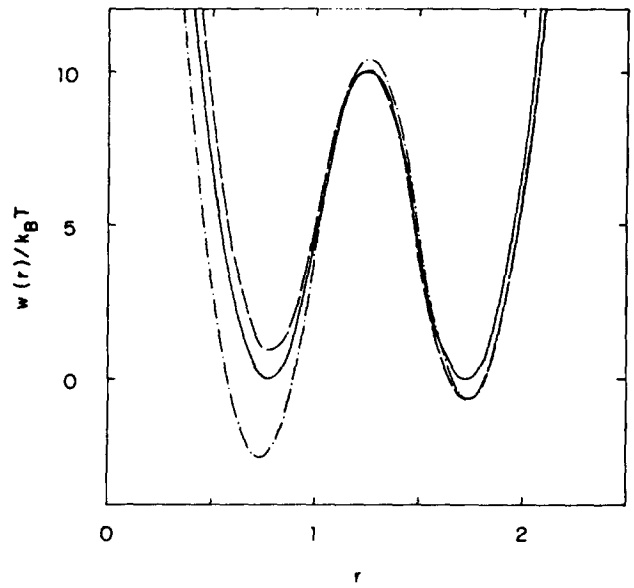

FIG. 7. The (—) bare potential, the bare potential plus the rotational contribution (– –), and the bare potential plus the rotational and solvent contributions (–·–), for the isomerizing diatomic molecule solvated in a simple Lennard-Jones fluid of density $\rho = 1.05$.

$$\Delta W_{\text{eff}}(r) = \Delta W(r) - 2k_B T \ln\left(\frac{r}{a}\right) \tag{3.8}$$

which includes the centrifugal distortions due to rotation of the diatomic. Figure 7 shows separately the contributing terms and the overall potential of mean force for the reduced solvent density $\rho = 1.05$.

For our diatomic system, the *gas phase* transition state theory rate constant is approximately

$$k_{\text{TST}}^{\text{in}\to\text{out}} \approx \left(\frac{a}{r_1}\right)^2 k_{\text{TST}}^{\text{1D}}, \tag{3.9}$$

$$k_{\text{TST}}^{\text{out}\to\text{in}} \approx \left(\frac{a}{r_2}\right)^2 k_{\text{TST}}^{\text{1D}}. \tag{3.10}$$

The prefactor of each rate constant is due to the Jacobian in spherical coordinates where it is assumed that the probability distribution is strongly peaked at the potential minina of the inner, r_1, and outer, r_2, wells. The gas phase potential is given by Eq. (3.2). The corresponding equilibrium constant is

$$K_{\text{eq}}^{\text{gas}} \approx \left(\frac{r_2}{r_1}\right)^2. \tag{3.11}$$

Figure 8 shows the behavior of the equilibrium constants $K_{\text{eq}} = X_{\text{out}}/X_{\text{in}}$ and the forward and backward transition state rate constants as a function of the solvent density, normalized by the gas phase constants [Eqs. (3.9), (3.10), and (3.11)]. With the parameters $a = 1.25$, $\beta Q = 10$, and $\hat{T} = 2.5$ we find for the gas phase, that the internal potential parameters $\omega_B = 15$ and $\omega_0 = 30$ correspond to $k_{\text{TST}}^{\text{in}\to\text{out}} = 1.33\times10^{-3}$, $k_{\text{TST}}^{\text{out}\to\text{in}} = 8.51\times10^{-5}$, and $K_{\text{eq}}^{\text{gas}} = 15.6$; for $\omega_B = 30$ and $\omega_0 = 30$ we find $k_{\text{TST}}^{\text{in}\to\text{out}} = 5.59\times10^{-4}$, $k_{\text{TST}}^{\text{out}\to\text{in}} = 1.14\times10^{-4}$, and $K_{\text{eq}}^{\text{gas}} = 4.89$. For our reaction system, we find, as expected, that at higher solvent densities the contracted state of the molecule will be favored over the extended state which displaces a larger volume. This trend is quantitatively displayed.

C. Transmission coefficient

The transmission coefficient κ, a dynamic quantity, is related to the normalized reactive flux[45] can be expressed as[47]

$$\hat{k}(t) = \langle \theta[q(t)] \rangle_+ - \langle \theta[q(t)] \rangle_-, \tag{3.12}$$

where $\theta(q)$ is the Heaviside function, which is unity for $q > 0$ and zero otherwise, and $\langle \cdots \rangle_\pm$ indicate, respectively, averages over the normalized phase space distribution functions[47]

$$P^{(\pm)}(\Gamma) = \frac{\dot{q}\theta(\pm\dot{q})\delta(q)e^{-\beta H(\Gamma)}}{\int d\Gamma\, \dot{q}\theta(\pm\dot{q})\delta(q)e^{-\beta H(\Gamma)}}, \tag{3.13}$$

where quantities without an explicit time variable are taken at the time origin.

If the barrier separating the reactant and product states is high $Q \gg k_B T$, $\hat{k}(t)$ will decay on two distinct time scales.[45] A fast initial decay will be followed by a slow decay, on the order of $e^{\beta Q}$,

$$\hat{k}(t) \to \kappa e^{-kt} \tag{3.14}$$

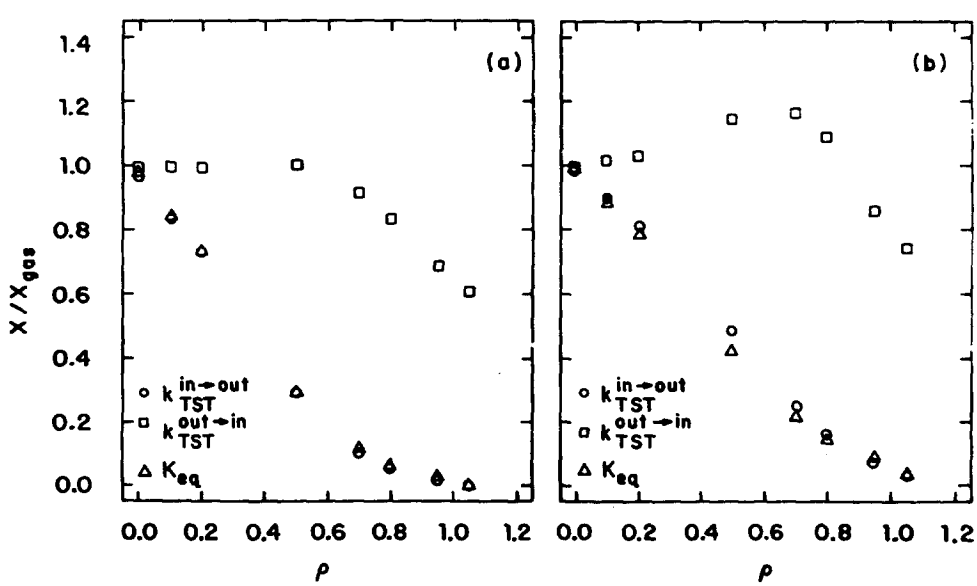

FIG. 8. The gas phase normalized equilibrium constant and transition state rate constants for the isomerizing diatomic calculated through the potential of mean force in Fig. 7 and Eq. (3.7). The system parameters are $\beta Q = 10$ and $\hat{T} = 2.5$ in each figure while in (a) $\omega_B = 15$, $\omega_0 = 30$; (b) $\omega_B = 30$, $\omega_0 = 30$.

from a "plateau value" which is the transmission coefficient κ.[5]

Straub and Berne have proposed the absorbing boundary method for determining the transmission coefficient, which is valid if the distribution of those trajectories which recross the transition state conforms to the distribution of Eq. (3.13).[48] In such a case, the transmission coefficient may be written

$$\kappa = \frac{T_+ T_-}{T_+ + T_- - T_+ T_-}, \tag{3.15}$$

where T_+ and T_- are, respectively, the probability that a trajectory starting at the transition state, distributed according to Eq. (3.13), will be trapped in the reactant or product state for times on the order of $e^{\beta Q}$ before recrossing.

To calculate the trapping fractions $T_\pm$ one samples points according to Eq. (3.13) which places trajectories initially at the transition state with $+$ ($-$) velocity, heading for the product (reactant) well. Each trajectory is propagated until it recrosses the transition state, at which point it is removed. If we define the survival probability $P_\pm(t)$ as the fraction of trajectories which has not crossed the transition state by time t, then $P_\pm(t)$ will decay to the plateau value $T_\pm$. If $k \ll k_{\mathrm{TST}}$, $\kappa \ll 1$, the trapping fraction will be small, and very few trajectories will have to be integrated for the full length of the simulation. In this case, the absorbing boundary method requires far less computer time than a full reactive flux calculation.[48]

D. Initial conditions

The initial distribution of states used in the calculation of the transmission coefficient is defined by Eq. (3.13) where the reaction coordinate is confined to the transition state. When the reaction coordinate is simply defined in terms of some separable coordinate, such as a linear combination of Cartesian coordinates or the radial component of spherical coordinates, the average of the velocities and coordinates can be separated and the transition state theory rate of Eqs. (3.4) and (3.5) is simply[47]

$$k_{\mathrm{TST}}^{\mathrm{in}\to\mathrm{out}} = \frac{1}{X_{\mathrm{in}}}\langle \dot{q} \rangle S(q), \tag{3.16}$$

$$k_{\mathrm{TST}}^{\mathrm{out}\to\mathrm{in}} = \frac{1}{X_{\mathrm{out}}}\langle \dot{q} \rangle S(q), \tag{3.17}$$

where $S(q)$ may be defined in terms of the potential of mean force $w(q)$[36] as[49]

$$S(q_0) = \langle \delta(q - q_0) \rangle = \frac{e^{-\beta w(q_0)}}{\int_0^\infty dq\, e^{-\beta w(q)}} \tag{3.18}$$

which is simply the probability distribution function of q in a canonical ensemble. However, in general q is a curvilinear coordinate, and the average of the positions and velocities cannot be separated, as for example in butane.[14,31]

For our system, the reaction coordinate is the radial distance separating the atoms of the diatomic, and so the averages of the positions and velocities may be performed separately. In this case, it would be most simple to use Monte Carlo[47–50] or the SHAKE molecular dynamics algorithm[51] to generate the positions and then assign the velocities randomly according to the Maxwell distribution weighted by the reaction coordinate velocity. However, we chose to employ a general Monte Carlo scheme which does not make use of this fact.[31] It may be used to generate a distribution according to Eq. (3.13) for a general curvilinear reaction coordinate.

The initial system configuration is denoted α, with total potential and kinetic energy E_α, reaction coordinate velocity $\dot{q}_\alpha$, and probability $p_\alpha = |\dot{q}_\alpha| e^{-\beta E_\alpha}$. After a move, the new system energy is $E_{\alpha'}$ with probability $p_{\alpha'} = |\dot{q}_{\alpha'}| e^{-\beta E_{\alpha'}}$. If the probability $p_{\alpha'} \geq p_\alpha$ the move is accepted. Otherwise, a random number between zero and one is generated and if the number is greater than the ratio $p_{\alpha'}/p_\alpha$ the move is accepted.

Initially, the interparticle separation of the diatomic was fixed at the barrier maximum for the potential of mean force. The system was then equilibrated over 1000 passes using a traditional Metropolis algorithm sampling coordinates only to generate an equilibrium Boltzmann distribution. The solvent atom moves consisted of generating a random translation of the coordinates according to a uniform distribution within a cube. The dimension of the cube was chosen to produce an acceptance ratio of 0.5.

Velocities were then Monte Carlo sampled according to the weighted distribution of Eq. (3.13). The position and velocity of each solvent atom was translated uniformly within a cube. The moves for the diatomic molecule were of two types. First, the center of mass position and velocity of the rotor was moved, as if it were a solvent atom. Second, the positions and velocities of the two atoms of the diatomic were moved independently, as if they were each solvent atoms, and then they were moved together along the interparticle separation to satisfy the distance constraint. This allows for both translations and rotations of the constrained diatomic. The move sizes for the solvent, diatomic center of mass, and separate atom and diatomic were chosen to produce an acceptance ratio of 0.5 in each case.

To equilibrate the positions and velocities according to the distribution of Eq. (3.13), 1000 passes were taken. Afterwards, a trajectory was generated. Configurations to be used in the calculation of the transmission coefficient were separated by 100 passes. The distributions were then compared with Eq. (3.13) and found to be in excellent agreement.

E. Results

Our calculations of transmission coefficients for the isomerization of the diatomic molecule were performed on a Cray XMP-48. In each case, we employed the absorbing boundary method using the velocity Verlet algorithm with a time step of 2×10^{-3}. The results are displayed in Table II. For each system $\hat{T} = 2.5$ and $a = 1.25$; ρ is the number density of the solvent and diatomic system; NP is the total number of atoms including the reacting diatomic; λ, Q, and ω_B are potential parameters; m_{A^*} is the solute atomic mass; NT is the number of trajectories in each calculation of a trapping coefficient $T_\pm$; $t_{\max}$ is the total time over which the trajectories were propagated. We have calculated the transmission coefficient as a function of the solvent density for four systems, described below. The barrier frequency and solvent/solute mass ratio of each system were chosen to examine

TABLE II. Data from rate constant simulations.

ρ	NP	λ	Q	ω_B	m_{A^*}	NT	T_+	T_-	t_{max}
0.005	32	0.5	25.0	15.0	1.0	1000	0.034	0.011	200.0
0.05	64	0.5	25.0	15.0	1.0	500	0.226	0.156	20.0
0.5	512	0.5	25.0	15.0	1.0	100	0.900	0.790	1.0
1.0	512	0.5	25.0	15.0	1.0	100	0.590	0.760	1.0
0.005	32	1.0	25.0	30.0	1.0	1000	0.025	0.011	200.0
0.05	64	1.0	25.0	30.0	1.0	500	0.172	0.172	20.0
0.5	512	1.0	25.0	30.0	1.0	100	0.870	0.880	1.0
1.0	512	1.0	25.0	30.0	1.0	100	0.760	0.860	1.0
0.005	32	0.5	25.0	15.0	0.1	1000	0.025	0.010	1000.0
0.05	64	0.5	25.0	15.0	0.1	500	0.152	0.106	100.0
0.5	512	0.5	25.0	15.0	0.1	100	0.930	0.790	5.0
1.0	512	0.5	25.0	15.0	0.1	100	0.770	0.910	5.0
0.005	32	1.0	25.0	30.0	4.0	1000	0.017	0.012	200.0
0.05	64	1.0	25.0	30.0	4.0	500	0.188	0.110	20.0
0.5	512	1.0	25.0	30.0	4.0	100	0.800	0.800	2.5
1.0	512	1.0	25.0	30.0	4.0	100	0.780	0.820	1.0

particular limits of interaction between the solvent and the reaction system. Below we describe each system separately.

1. Theoretical predictions

At *low friction*, the rate limiting step for the isomerization reaction will be energy activation. Collisions are rare and the rate will increase in proportion to the collision rate or friction.

If the energy transferred on collision between a solvent atom and the reaction coordinate is small compared to the thermal energy k_BT, a *weak collision model* is most appropriate[12]; the dynamics are modeled by the generalized Langevin equation

$$\mu\ddot{q} = \frac{-\partial w(q)}{\partial q} - \int_0^t dt'\,\zeta(t')\dot{q}(t-t') + R(t), \tag{3.19}$$

where q is the reaction coordinate, $\dot{q}$ the conjugate velocity, $\zeta(t)$ the dynamic friction on the reaction coordinate, and $R(t)$ the random force which satisfies the second fluctuation–dissipation theorem $\langle R(t)R(0)\rangle = \mu k_BT\zeta(t)$.

The rate for energy activation of the reaction coordinate to the barrier energy Q has been shown by Grote and Hynes[6] to be approximately

$$k_{wc} \approx \frac{\mathrm{Re}\,\hat{\zeta}(-i\omega_0)}{2}\beta Q e^{-\beta Q} \tag{3.20}$$

for $\beta Q \gg k_BT$ and a harmonic well of frequency ω_0. In the adiabatic limit, the solvent relaxes quickly and follows the motion of the reaction coordinate. The friction felt by the reaction coordinate is the integrated or zero frequency friction and Eq. (3.20) reduces to the Kramers rate for energy activation

$$k_{wc}^K \approx \frac{\zeta}{2}\beta Q e^{-\beta Q}, \tag{3.21}$$

where $\zeta = \hat{\zeta}(0)$.

If the energy transferred on collision to the reaction coordinate is comparable to or larger than the thermal energy a strong collision model like the *BGK impulsive collision model* is appropriate[5]; the dynamics is described by a master equation where each collision of the reaction coordinate with a solvent atom is assumed to thermalize the reaction coordinate velocity, while leaving the position constant. The rate for energy activation is almost equal to the strong collision approximation, i.e.,[4]

$$k_{BGK} \approx \frac{\alpha}{2}e^{-\beta Q}, \tag{3.22}$$

where α is the collision frequency experienced by the reaction coordinate. *It should be noted that the strong collision approximation gives the upper limit for the rate constant for energy activation.*[11,23] *Therefore, the smaller of the two rate constants given by Eqs. (3.22) and (3.20) will be rate limiting.*

At *high friction*, the rate limiting step for the isomerization reaction will be motion through the transition state (barrier) region. Collisions are frequent and the reaction coordinate is assumed to have a thermal distribution of states up to and including the barrier energy. Deviations from transition state theory occur if the motion of the reaction coordinate through the barrier region is hindered; that is, there are multiple rapid barrier recrossings.

Grote and Hynes have shown that the rate constant for crossing the saddle region with parabolic barrier of frequency ω_B is given by[27]

$$k_{GH} = \frac{\lambda_r}{\omega_B}k_{TST}, \tag{3.23}$$

where the reactive frequency λ_r is the positive solution of the equation

$$\lambda_r^2 + \lambda_r\hat{\zeta}(\lambda_r) = \omega_B^2. \tag{3.24}$$

In the adiabatic limit where the bath relaxes quickly compared to the solute the zero frequency friction $\hat{\zeta}(0)$ will be a good approximation to the friction on the reaction coordinate and $\hat{\zeta}(0) \gg \omega_B$. Equation (3.23) then reduces to the Kramers rate for the diffusive crossing of a parabolic barrier

$$k_{diff} \approx \frac{\omega_B}{\zeta}k_{TST} \tag{3.25}$$

in the limit of large ζ.

Similarly, the BGK impulsive collision model results in Eq. (3.25) where the collision frequency α is substituted for the zero frequency friction ζ.

To bridge between the low and high friction limits, and provide a functional form for the total rate constant k for all friction or collision frequency, it is necessary to use approximate connection formulas. For the weak collision models we use[12]

$$k^{-1} \approx k_{wc}^{-1} + k_{GH}^{-1} \tag{3.26}$$

which also applies approximately in the adiabatic Kramers limit. For the impulsive collision model we use[52]

$$k^{-1} \approx k_{BGK}^{-1} + k_{TST}^{-1} + k_{diff}^{-1}. \tag{3.27}$$

2. Simulation results

In this section we present simulation results for four different systems together with the predictions of those theories presented in Sec. III E 1. A detailed discussion of the application of the theories and the significance of their agreement with the simulation results is given in Sec. IV. In Fig. 9 we plot the absolute rate constants for the forward and back-

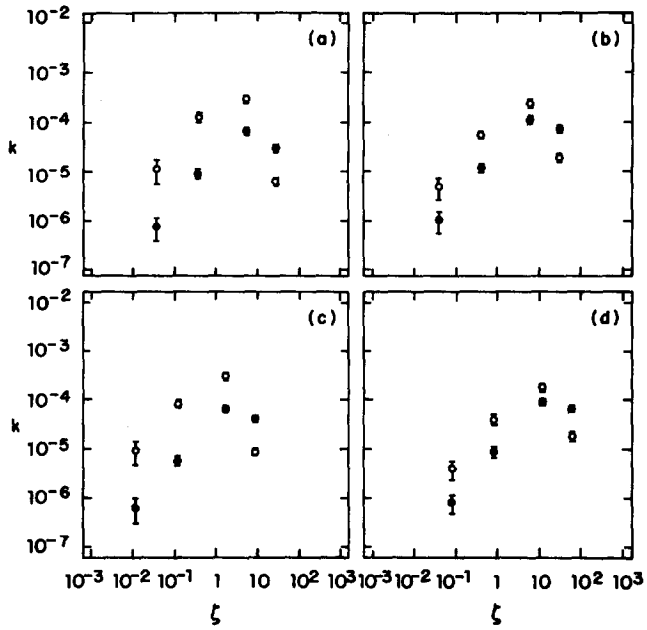

FIG. 9. $k^{\text{in}\to\text{out}}$ (○) and $k^{\text{out}\to\text{in}}$ (●) absolute rate constants as a function of the solvent density, expressed here as the zero frequency friction of the solvent ζ. The system parameters are $\beta Q = 10$ and $\hat{T} = 2.5$ in each figure while in (a) $m_A/m_{A^*} = 1.0$, $\omega_B = 15$, $\omega_0 = 30$; (b) $m_A/m_{A^*} = 1.0$, $\omega_B = 30$, $\omega_0 = 30$; (c) $m_A/m_{A^*} = 0.1$, $\omega_B = 15$, $\omega_0 = 30$; (d) $m_A/m_{A^*} = 4.0$, $\omega_B = 30$, $\omega_0 = 30$.

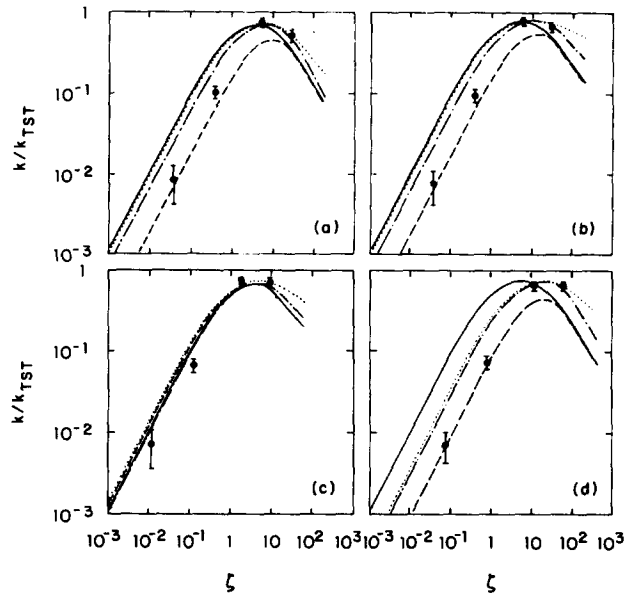

FIG. 10. The transmission coefficient as a function of the solvent density, expressed here as the zero frequency friction of the solvent ζ. The theoretical predictions of the Kramers theory (—), the BGK theory (– –), the weak collision model using the single particle approximation to the reaction coordinate friction (···) (see Sec. IV C), and an exponential approximation to the friction (–·–) using the correlation time of Eq. (2.9). The system parameters are $\beta Q = 10$ and $\hat{T} = 2.5$ in each figure while in (a) $m_A/m_{A^*} = 1.0$, $\omega_B = 15$, $\omega_0 = 30$; (b) $m_A/m_{A^*} = 1.0$, $\omega_B = 30$, $\omega_0 = 30$; (c) $m_A/m_{A^*} = 0.1$, $\omega_B = 15$, $\omega_0 = 30$; (d) $m_A/m_{A^*} = 4.0$, $\omega_B = 30$, $\omega_0 = 30$.

ward reactions [cf. Eq. (3.3)] as a function of the zero frequency friction $\zeta = \hat{\zeta}(0)$ of the solvent. In Fig. 10 we plot the transmission coefficient as a function of the zero frequency friction of the solvent $\zeta = \hat{\zeta}(0)$. Note the different appearance of the absolute rate constants (Fig. 9) which would be observed in an experiment and the transmission coefficient (Fig. 10) which can be meaningfully compared to dynamical theories. These differences arise from the potential of mean force (solvent shifts). In this example, it is quite obvious that without detailed knowledge of the potential of mean force effect a meaningful comparison with dynamical theories is impossible. Unfortunately, examples of such analyses of experimental data are quite uncommon in the literature.

In *system 1,* the barrier frequency $\omega_B = 15$ was chosen to be lower than the dominant solvent frequency $\omega_{\text{solvent}} \approx 30$. Here it is expected that the solvent will respond nearly adiabatically to the motion of the reaction coordinate as it moves through the transition region. Figure 10(a) compares the simulation results with various theoretical predictions.

At low density and friction, the rate constants show good agreement with the BGK theory. As the density is increased the maximum in the rate constant and the initial fall off agree with the nonadiabatic weak collision theory which uses the full memory kernel (see Sec. IV C).

In *system 2,* the barrier frequency $\omega_B = 30$ was chosen to be comparable to the dominant solvent frequency. Here it is expected that the solvent will have difficulties responding adiabatically to the motion of the reaction coordinate. There should be a definite separation between the adiabatic Kramers and the nonadiabatic Grote–Hynes rate constants. Figure 10(b) compares the simulation results with various theoretical predictions.

At low density, the rate constants show good agreement with the BGK theory. As the density is increased the maximum in the rate constant and the initial fall off agree with the weak collision theory using the full memory kernel.

In *system 3,* the barrier frequency $\omega_B = 15.0$ was chosen to be less than the dominant solvent frequency, and the mass of the solvent was decreased to $m_A = m_{A^*}/10$ to increase the solvent response. Here it is expected that the solvent will respond nearly adiabatically to the motion of the reaction coordinate as it moves through the transition region. Figure 10(c) compares the simulation results with the theoretical predictions.

At low density, the rate constants sit slightly below all theoretical predictions. As the density is increased the maximum in the rate constant and the initial falloff agree with the nonadiabatic Grote–Hynes theory which is closely approximated by the adiabatic Kramers weak collision theory which uses the zero frequency friction.

In *system 4,* the barrier frequency $\omega_B = 30$ is comparable to the dominant solvent frequency, and the mass of the solvent was increased to $m_A = 4m_{A^*}$ to impede the solvent response. Here it is expected that the solvent will have difficulties responding to the motion of the reaction coordinate. Figure 10(d) compares the simulation results with the theoretical predictions.

At low density, the rate constants are in excellent agreement with the BGK theory. The turnover region and high density falloff occur at a higher density than with the lighter solvent of *system 3* and agree well with the nonadiabatic Grote–Hynes theory using the full memory (see Sec. IV C).

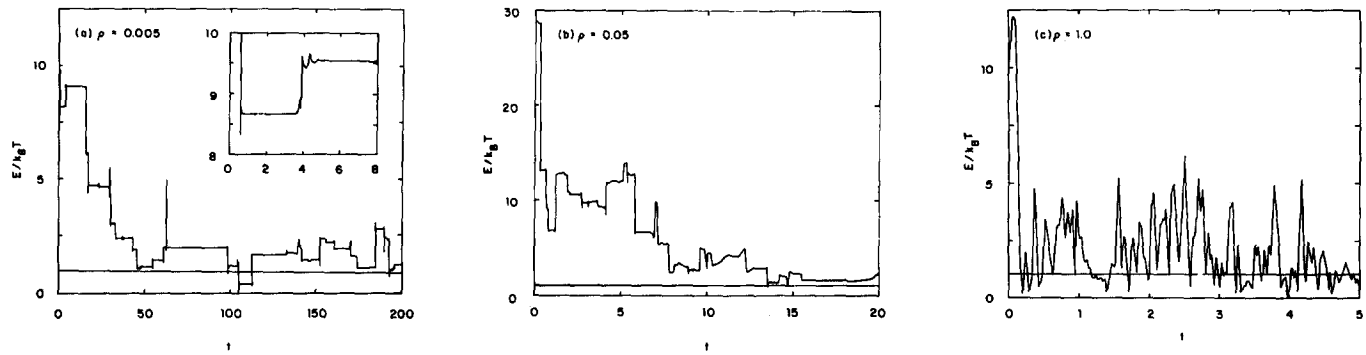

FIG. 11. The behavior of the reaction coordinate is described by trajectories at reduced solvent densities of $\rho =$ (a) 0.005; (b) 0.05; and (c) 1.0.

IV. ANALYSIS OF RATE DATA

To understand deviations between experimental results, including those of complex simulations, and theoretical predictions it is important to determine first, if the dynamic model is appropriate, second, if the basic assumptions of the theory which connect the dynamic model with the rate constant are valid for that system, and third, if the parameters required as input are known accurately.

Molecular dynamics simulation can be effectively used to examine dynamic trajectories and decide if their motion is well modeled by the basic equations of motion used in the theory, e.g., if the collisional energy transfer is best described by a weak or impulsive collision model. Further, stochastic dynamics can be used to simulate the chosen collisional model and generate rate constants to test the basic theoretical assumptions which connect the equations of motion with the kinetic rate constant. If all assumptions are met, then the theory is compared to the experimental results to address the validity of the model or the accuracy of required parameters.

In this section we examine the details of collisional energy transfer and find that for the equal mass system at low collision frequency the microscopic dynamics are best described by an impulsive collision model, rather than the weak collision Langevin model. We also present the results of stochastic simulations for the isomerization of the diatomic molecule. For the BGK impulsive collision model, and weak collision models using zero frequency and exponential dynamic friction models, we find that the theoretical predictions of Eqs. (3.26) and (3.27) are accurate. Finally, we examine the validity of using an approximation to the reaction coordinate friction based on the single particle friction.

A. Collisional parameters

For the isomerizing diatomic molecule we would like to know the frequency of collisions with the solvent α and the average energy transfer on collision, $|\langle \Delta E \rangle|$.

Figure 11 shows the reaction coordinate energy as a function of time for activated trajectories which begin just above the barrier and are propagated in solvents of different density. At low density, $\rho = 0.005$, the collisions are binary, abrupt, and the energy transfer is likewise. Occasionally, a collision complex is formed which is indicated by a spike and adjacent "ringing" in the energy [see insert of Fig. 11(a)]. There are also large spikes from elastic collisions with no resultant energy transfer. At $\rho = 0.05$, individual, binary collisions are difficult to resolve. However, there remain large abrupt transfers of energy. By $\rho = 1.0$, the changes in energy are continuous in time and the energy is diffusive.

We have examined 175 activated trajectories, distributed according to Eq. (3.13), at a density of $\rho = 0.005$. The diatomic potential parameters are $\omega_B = 30$, $\lambda = 1$, $\beta Q = 10$, $\hat{T} = 2.5$, and $m_A = m_{A^*}$.

For each trajectory we measured the time between initialization and first collision as well as the energy transferred. The resulting distributions of times and energies are displayed in Fig. 12. The collision times are well described by an exponential distribution with decay constant, corresponding to the average collision time $\langle \Delta t \rangle = 5.0$. The two wings of the energy distribution, corresponding to increases and decreases in energy, may be fit by exponentials. The average increase in energy is $\langle \Delta E \rangle_+ = 0.24 k_B T$, the average decrease in energy is $\langle \Delta E \rangle_- = -1.56 k_B T$, and the average energy change on collision is $\langle \Delta E \rangle = -1.32 k_B T$. The exponential distribution displayed in Fig. 12(b) for collisional energy change is simply proportional to $\exp[(E - E')/\langle \Delta E \rangle_\pm]$.

The average collisional energy transfer at low density is greater than the thermal energy $k_B T$ indicating that the impulsive collision models, such as the BGK or strong collision, are the best dynamic models for this system.

We can compare the average collision time $\langle \Delta t \rangle$ with that predicted by kinetic theory. The collision frequency for our diatomic molecule A_2^* in a monatomic solvent of atoms A can be approximated from the collision frequency of an impurity in a Lennard-Jones gas[53,54]

$$Z_{LJ} = \rho \pi \sigma^2_{A_2^*-A} \sqrt{8 k_B T/\pi \mu_{A_2^*-A}}\, \Omega^{(2,2)^*}. \tag{4.1}$$

ρ is the solvent density, $\sigma_{A_2^*-A}$ is the collision diameter for the binary collision, $\mu_{A_2^*-A}$ is the reduced mass of the collision pair, and $\Omega^{(2,2)^*}$ is the reduced collision integral.

For two spherical Lennard-Jones atoms $\sigma_{A_2^*-A} = (\sigma_{A_2^*} + \sigma_A)/2$. We can approximate the collision diameter of the diatomic molecule by averaging the cross section seen by a solvent atom moving along each of the three axes of the diatomic and assuming that each collision between the solvent and the solute is a collision with the reaction coordinate. Neglecting rotations, the area (in units of $\pi \sigma_A^2/4$) of the

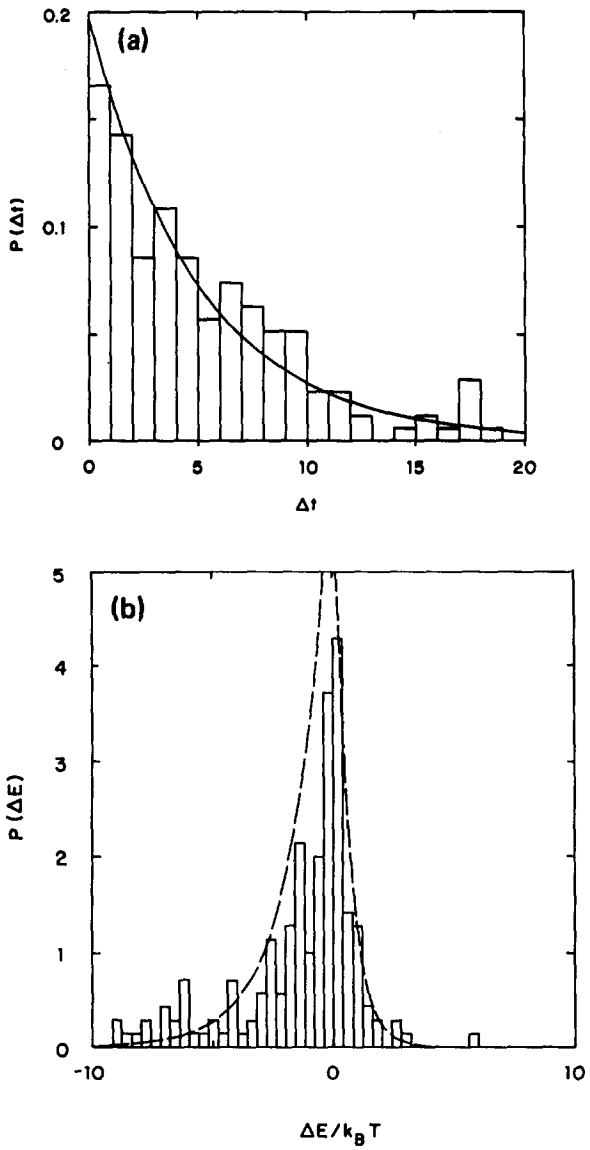

FIG. 12. The probability of (a) the collision time Δt and (b) the average energy transfer on collision ΔE of a solvent atom with an activated diatomic molecule. The envelopes are exponential fits to the data.

diatomic projected onto the plane perpendicular to the reaction coordinate is unity, while the area projected onto each plane containing the reaction coordinate of length $r = a$ is $2 - [2\cos^{-1}(a/2) - a(1 - a^2/4)^{1/2}]/\pi$.[55] Averaging the three projections for the transition state separation $r = a = 1.25$ gives $\sigma_{A_2^\ddagger} \approx 1.21$ and $\sigma_{A_2^\ddagger - A} \approx 1.10$.

The reduced mass $\mu_{A_2^\ddagger - A} = 2/3$ and the reduced collision integral at $\hat{T} = 2.5$ is $\Omega^{(2,2)*} = 1.093$.[53] Using the low density approximation from Eq. (2.7), $\rho \approx \hat{\zeta}(0)/7.47$, results in $Z_{LJ} \approx 1.72\hat{\zeta}(0)$ assuming slow rotations. We emphasize that this estimate of the collision frequency is approximate, but adequate for our analysis.[67]

We noted earlier that the BGK rate constant agrees well with the numerical rate constants at low densities. To better appreciate this agreement, we calculate the collision efficiency β_c which we define in terms of the measured rate constant k and the BGK rate constant k_{BGK} as

$$k = \beta_c k_{BGK} . \tag{4.2}$$

Following Troe,[54] we further divide the collision efficiency as $\beta_c = \beta_{c\sigma}\beta_{c\Delta E}$, into a "step size factor"

$$\beta_{c\Delta E} = \left[\frac{\langle \Delta E \rangle_-}{k_B T - \langle \Delta E \rangle_-}\right]^2 \tag{4.3}$$

which reflects the efficiency of energy transfer per collision, and a "total cross section factor"

$$\beta_{c\sigma} = \frac{Z_{sim}}{Z_{LJ}} \tag{4.4}$$

which reflects the accuracy of the kinetic theory approximation for the collision frequency. In the strong collision limit, the average energy transfer per collision $|\langle \Delta E \rangle_-| \gg k_B T$ and $\beta_{c\Delta E} = 1$.

Our simulation results in an average collisional energy transfer of $\langle \Delta E \rangle_- = -1.56 k_B T$. The average collision time is $\langle \Delta t \rangle = 5.0$ at a density of $\rho = 0.005$ which gives a collision frequency of $Z_{sim} \approx 5.35\hat{\zeta}(0)$. As a result, $\beta_{c\Delta E} = 0.37$, $\beta_{c\sigma} = 3.11$, and $\beta_c = 1.15$. The good agreement between the simulation and BGK theory for *systems 1* and *2* is the result of a compensation of errors. The kinetic theory result overestimates the actual collision frequency by a factor of 3. This is probably due to an energy dependence of the collision frequency. The energy transfer, on the other hand, is a factor of 3 less efficient than required by a strong collision model.

Table III summarizes the data taken for collisional energy transfer of 100 trajectories for two additional values of the ratio of solvent to solute mass corresponding to the parameters of *systems 3* and *4*. For the system with heavy solvent, $m_A/m_{A^*} = 4.0$, the resulting values agree very well with the expectations of an exponential model.[54,56] Figure 10(d) shows that for this mass ratio the Langevin and BGK predictions are well separated. The simulation data shows best agreement with the BGK model.

For the system with light solvent, $m_A/m_{A^*} = 0.1$, because of the small transfer of energy it was more difficult to define a collision. However, the data does display the expected trends, and results in a collision efficiency substantially less than one, even with the overestimate of the kinetic theory result for the collision frequency. In Fig. 10(c) there is less separation between the BGK and Langevin predictions. As the solvent mass is reduced, the reduced mass of the solvent–diatom collision pair decreases and the collision frequency increases. Conversely, as the solvent mass is reduced the zero frequency friction decreases, roughly as the square root of the solvent mass. For this light solvent the BGK theory prediction is close to that of the weak collision theories, each of which show reasonable agreement with the simulation results. However, Table III shows that the collision

TABLE III. Collision energy transfer data.

m_A/m_{A^*}	$\langle \Delta t \rangle$	$\langle \Delta E \rangle_-$	$\langle \Delta E \rangle_+$	$\beta_{c\sigma}$	$\beta_{c\Delta E}$	β_c
1.0	5.0	−1.56	0.24	3.1	0.37	1.1
4.0	4.6	−2.85	0.73	4.8	0.55	2.6
0.1	3.1	−0.78	0.16	1.9	0.19	0.4

efficiency is low indicating that the agreement is coincidental. If we were to lower the solvent mass further we could expect the BGK theory prediction will lie well above the predictions of the weak collision model and that the rate data would show agreement with the rate limiting weak collision theory.

B. Model systems

In this section, we test the validity of the connection formulas, Eqs. (3.26) and (3.27).

We have used the absorbing boundary approximation to the reactive flux[48] to calculate transmission coefficients as a function of the collision frequency or friction for a barrier height of $\beta Q = 10$, a barrier frequency $\omega_B = 30$, well frequency $\omega_0 = 30$, and a transition state surface located at $r = 1.25$. These parameters correspond to *systems 2* and *4*.

The BGK impulsive collision model requires that at random times, sampled from a Poisson distribution, the velocity of the trajectory is randomized according to a thermal distribution. Between collisions the trajectory is propagated according to Newton's equations of motion.[5] Trajectories were propagated using the velocity Verlet algorithm with a time step of 2×10^{-3} on an FPS-164 attached processor.

Figure 13 compares the stochastic simulation results with the connection formula, Eq. (3.27). The simulation results show perfect agreement with the theoretical predictions in the limits of low and high α. There is a small deviation at intermediate α. These results indicate that the assumptions implicit in Eq. (3.27) are satisfied for this potential and choice of system parameters.

The weak collision generalized Langevin model is simulated according to the equation of motion, Eq. (3.19). This is readily done for constant friction $\zeta(t) = 2\zeta\delta(t)$ and exponential friction $\zeta(t) = \zeta e^{-t/\tau_c}/\tau_c$ where $\zeta = \hat{\zeta}(0)$. The details of such simulations have been described elsewhere.[32,48]

Figure 14 compares the stochastic simulation results for exponential friction with the connection formula, Eq.

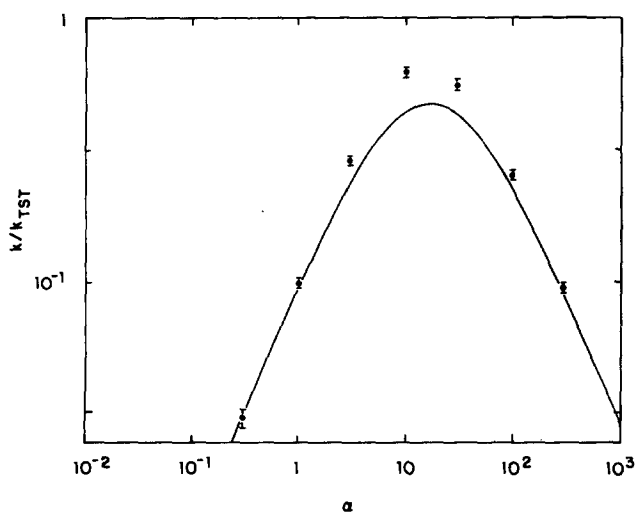

FIG. 13. The transmission coefficient for the isomerization reaction is shown as a function of the collision frequency α where the dynamics are defined by the impulsive BGK collision model. The solid line is the prediction of the BGK theory, Eq. (3.27).

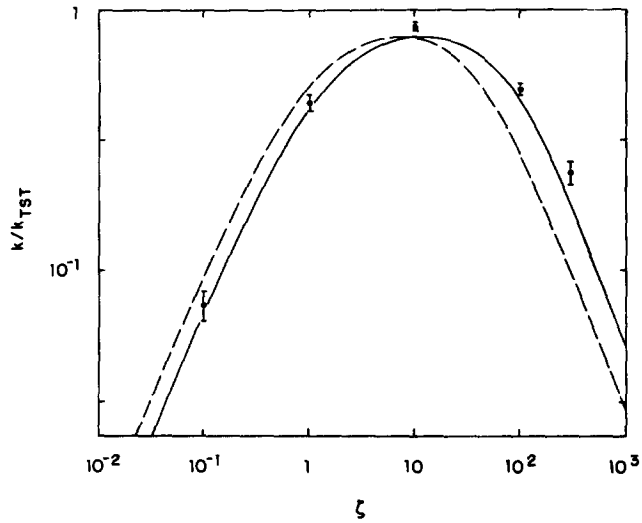

FIG. 14. The transmission coefficient for the isomerization reaction is shown as a function of the zero frequency friction ζ. The dynamics are defined by the generalized Langevin equation with an exponential form of the dynamic friction. The solid line is the prediction of the weak collision theory using the exponential friction, Eq. (3.26), while the dashed line is the prediction of Kramers theory, Eq. (3.26).

(3.26). The parameter τ_c, the correlation time of the solvent, is given by Eq. (2.9). There is good agreement with the theoretical predictions over the entire range of ζ. There is no indication of a breakdown in the connection formula, Eq. (3.26), in agreement with the limits proposed for its validity.[13,32,57]

For each of the model calculations, which grant the validity of the dynamic model, the theoretical predictions of Eqs. (3.26) and (3.27) show good agreement with the simulation results.

C. Reaction coordinate friction

The dynamic friction used in the generalized Langevin equation [Eq. (3.19)] has several important properties. The initial time value $\zeta_r(0)$ is independent of the mass of the solvent.[36] Additionally, for an anharmonic oscillator linearly coupled to a harmonic bath a change in the mass of the solvent will cause a change in the time scale of the decay of the friction, but will not change its structure.[21,58] In particular, the time appears as ωt where the frequency ω varies as the inverse of the square root of the solvent mass. The corresponding zero frequency friction will vary as the square root of the solvent mass.

In applying the weak collision theories in Figs. 10(a)–10(d) we have assumed that the friction on the reaction coordinate $\zeta_r(t)$ is related to the single particle friction $\zeta_s(t)$ of Eq. (2.6) by $\zeta_r(t) = \zeta_s(t)/2$. This assumption is based on the fact that for two particles moving independently with diffusion coefficient $D \approx 1/\zeta$ the interparticle separation will diffuse with coefficient $D_{12} \approx 2/\zeta$ and the friction felt is one-half the friction acting on a single particle. It is a rough assumption to extend this to time dependent friction, or the friction on two particles not in the independent diffusion limit, but it is the most obvious and simple approximation.

This assumption gives us a friction for the case of equal mass of solvent and solute atoms. For *systems 3* and *4* where

the solvent mass is varied, we have assumed that the equal mass friction can be scaled in time, by multiplying the time in Eq. (2.6) by the inverse square root of the solvent mass. This would be exact for a harmonic bath linearly coupled to an anharmonic oscillator.[21,58]

The generalized Langevin equation, Eq. (3.19), assumes that the friction experienced by the reaction coordinate is independent of the particular value of the reaction coordinate, i.e., that it is spatially independent. We have recently shown that for the system studied in this paper, namely a diatomic in a Lennard-Jones fluid, both the time structure and the zero frequency friction depend strongly on the interparticle separation of the diatomic. If one wishes to apply the Grote–Hynes theory to calculate the rate for barrier crossing, or the non-Markovian theory for energy activation, it is important to calculate the friction at the barrier top or in the well, respectively. Of course, it would be most satisfying to employ a theory which is based on a generalized Langevin equation with spatially dependent friction.[13]

With our method, the coordinate of interest x, which could be a generalized coordinate or angle, is restricted by a harmonic confining potential of frequency ω to a region centered at x_0. We may write a generalized Langevin equation for $q = x - x_0$ as

$$\mu\ddot{q} = -\int_0^t dt'\,[\,\mu\tilde{\omega}^2 + \zeta_r(t')\,]\dot{q}(t-t') + R(t)\,, \tag{4.5}$$

where $\langle q\rangle = 0$, $\tilde{\omega}^2 = k_B T/\mu\,\langle q^2\rangle$, and $\zeta_r(t)$ is the friction felt by the coordinate q. The complementary memory function equation is

$$\dot{C}_v(t) = -\int_0^t dt'\left[\tilde{\omega}^2 + \frac{\zeta_r(t')}{\mu}\right]C_v(t-t')\,, \tag{4.6}$$

where $C_v(t) = \langle\dot{q}(t)\dot{q}(0)\rangle/\langle\dot{q}^2\rangle$ is the velocity autocorrelation function. By calculating $C_v(t)$ and $\tilde{\omega}^2$ in a simulation and inverting Eq. (4.6) we can extract the friction on q for motion near the equilibrium position. There should not be a dependence of $\zeta_r(t)$ on ω. Furthermore, a large ω limits the motion of the coordinate so that the friction should accurately represent the friction at a point along q, rather than an average over a region.

We have calculated $\zeta_r(t)$ for the three ratios of solvent to solute mass discussed here at $\rho = 1.0$ and $\hat{T} = 2.5$ with the interparticle separation confined near the transition state separation $r = 1.25$. This allows us to determine the rate for barrier crossing in the case where the solvent and solute masses are equal and the rate for energy diffusion is large. Table IV summarizes this data. The Grote–Hynes rate constant using the reaction coordinate friction shows good agreement with the simulation data. The Kramers theory predictions are slightly less than those of the Grote–Hynes theory. The approximate reaction coordinate friction, one-half the single particle friction, has a zero frequency value which is in each case less than the reaction coordinate friction, but never more than 25%. Therefore, for this system it is important to calculate the reaction coordinate friction, but the simple approximation gives reasonable agreement. However, for systems with more complicated reaction coordinates, such as the dihedral angle of butane, it is more difficult to approximate the friction using single particle properties or hydrodynamic theories. In such cases, it will be important to calculate the reaction coordinate friction directly using the above method or something comparable.[59,60]

TABLE IV. Comparison between the exact reaction coordinate friction and the single particle friction approximation. The transmission coefficients correspond to the rate constants given by the nonadiabatic κ, and the adiabatic Kramers limit κ_K, of Eq. (3.26) using the exact reaction coordinate friction.

m_A/m_{A^*}	ω_B	$\hat{\zeta}_r(0)$	$\hat{\zeta}_s(0)/2$	κ_K	κ	κ_{sim}
1.0	30	18.8	14.5	0.60	0.68	0.67
1.0	15	18.8	14.5	0.43	0.53	0.50
4.0	30	29.5	29.1	0.50	0.59	0.67
0.1	15	5.5	4.6	0.65	0.72	0.72

V. CONCLUSIONS

In this study we present a calculation of rate constants in perhaps the simplest imaginable model for an isomerization reaction—a hypothetical diatomic molecule which isomerizes between shorter and longer bond length states. We have carried out a detailed study of the behavior of the absolute rate constants as well as transmission coefficients over a wide range of solvent densities and considered different cases where the mass of the solvent equals the mass of the solute atoms, as well as for heavy and light solvents. The major aim of this study was to obtain all necessary quantities which influence the rate constant, such as the potential of mean force, the friction on the reaction coordinate, and the energy exchange on and frequency of collisions, in order to compare the simulation results with available theories for chemical reactions. *In all cases studied we conclude: The present theoretical models of chemical reactions in gases and condensed media are able to predict—within a factor of 2—the simulated rate constants.* However, it is imperative to know several key quantities: the potential of mean force, the friction on the reaction coordinate, and the collision rate. Poor knowledge of these quantities will ultimately cause incorrect predictions of the rate constants. We would like to stress this point, as several studies where experimentally measured rate constants have been compared with theoretical models did not—in our view—pay sufficient attention to these points and have led to continuing controversy.[8,19,61,62–64] Reasonably good estimates of these quantities, in particular the potential of mean force or the friction on the reaction coordinate, are available in the case of diatomic recombination reactions only.[21,52] Unfortunately, for more complex reactions such questions are matters of controversy where it is likely that the only means of obtaining sufficient information is extended molecular dynamics simulations.

The present model system allows for the study of the energy activation between the strong collision and weak collision limit as well as the influence of the potential of mean force. We believe that similar molecular dynamics studies provide a convenient alternative to more detailed but elaborate scattering calculations.[65] This is especially true at low pressures where only a small number of bath gas molecules

are required, which makes such calculations very quick even on small computers.

At low density, for the equal mass case we find that the rate constant agrees well with the BGK impulsive collision model. When the solvent mass is increased the collisions are more effective in transferring energy and the behavior shifts further towards that of the impulsive collision model. The details of energy transfer agree well with the exponential model of Troe *et al.*[54] For the lighter solvent, the energy transfer is best described by a weak collision model. Our estimate of the collision rate, based on the atomic collision frequency for a simple Lennard-Jones system, overestimated the rate while the energy transfer efficiency was less than unity. These compensating effects explain the agreement between the simulation data and the BGK predictions.

On the other hand, the damping produced by the Lennard-Jonesium solvent is insufficient to produce large deviations from transition state theory at high densities. The differences between the predictions of transition state theory, Kramers theory, and Grote–Hynes theory do not differ markedly and lie within a factor of 2. Nevertheless, some conclusions from the present study can be drawn. It is clearly seen, that the predictions of the Grote–Hynes theory using the proper frequency dependent friction are superior to the simple Kramers model. Furthermore, to approximate the friction on the reaction coordinate by the single particle friction is a reasonable approximation in this case. For each ratio of solvent to solute mass the assumption that the reaction coordinate friction is one-half the single particle friction, with the time constants scaled by the inverse square root of the solvent mass, results in a zero frequency friction accurate to within 25% of the directly calculated friction. However, the strong spatial dependence of the reaction coordinate friction[21] cannot be reproduced. However, we do not think that these conclusions will necessarily apply to more complex reactions. In particular, the correlation times in the present case are not large enough to enter the regime of parameter space where severe deviations from all known theories are observed.[32] Other systems which include charge–dipole or dipole–dipole interactions,[60] or isomerization reactions which require large solvent displacements,[66] generate significantly higher friction on the reaction coordinate. On the other hand, the theoretical estimation of the friction on the reaction coordinate in those cases is much more problematic than in our system, where the single particle friction as well as the friction on the reaction coordinate have been evaluated accurately. It will be necessary to calculate the friction using molecular dynamics simulation.

In conclusion, the results of the present molecular dynamics study of a model chemical reaction in a realistic rare gas solvent as a function of density represents a novel challenge to our understanding of chemical rate processes in gases and liquids. In this case, we were able to predict the rate constant from simple models provided we knew the friction on the reaction coordinate and the potential of mean force. Detailed knowledge of these quantities is of key importance for the understanding of our system as well as experimentally studied systems. Unfortunately, in many realistic systems such quantities cannot be estimated with sufficient accuracy. Therefore, we believe that similar studies on more complicated reaction systems will prompt new developments in rate theory and at the same time lead to a detailed understanding of chemical reactions in condensed systems.

[1] S. Glasstone, K. J. Laidler, and H. Eyring, *The Theory of Rate Processes* (McGraw–Hill, New York, 1941).
[2] H. Eyring, J. Chem. Phys. **3**, 107 (1934).
[3] E. Wigner, J. Chem. Phys. **5**, 720 (1937).
[4] J. L. Skinner and P. G. Wolynes, J. Chem. Phys. **69**, 2143 (1978).
[5] J. A. Montgomery, Jr., D. Chandler, and B. J. Berne, J. Chem. Phys. **70**, 4056 (1979).
[6] R. F. Grote and J. T. Hynes, J. Chem. Phys. **77**, 3736 (1982).
[7] D. P. Millar and K. B. Eisenthal, J. Chem. Phys. **83**, 5076 (1985).
[8] D. L. Hasha, T. Eguchi, and J. Jonas, J. Am. Chem. Soc. **104**, 2290 (1982).
[9] G. R. Fleming, S. H. Courtney, and M. W. Balk, J. Stat. Phys. **42**, 83 (1986).
[10] M. Lee, G. R. Holtom, and R. M. Hochstrasser, Chem. Phys. Lett. **118**, 359 (1985).
[11] J. Troe, Annu. Rev. Phys. Chem. **29**, 223 (1978).
[12] J. T. Hynes, in *Theory of Chemical Reaction Dynamics*, edited by M. Baer (Chemical Rubber, Boca Raton, FL, 1985), p. 171.
[13] P. Hänggi, J. Stat. Phys. **42**, 105 (1985), addendum and erratum; **44**, 1003 (1986).
[14] B. J. Berne, M. Borkovec, and J. E. Straub, J. Phys. Chem. **92**, 3711 (1988).
[15] W. L. Jorgensen and J. K. Buckner, J. Phys. Chem. **91**, 4651 (1986).
[16] M. Dantus, M. J. Rosker, and A. H. Zewail, J. Chem. Phys. **87**, 2395 (1987).
[17] H. A. Kramers, Physica **7**, 284 (1940).
[18] J. L. Skinner and P. G. Wolynes, J. Chem. Phys. **72**, 4913 (1980).
[19] B. Bagchi and D. A. Oxtoby, J. Chem. Phys. **78**, 2735 (1983).
[20] G. van der Zwan and J. T. Hynes, J. Chem. Phys. **76**, 2993 (1982).
[21] J. E. Straub, M. Borkovec, and B. J. Berne, J. Phys. Chem. **91**, 4995 (1987).
[22] A convenient distinction of the approaches is possible with the Lindemann mechanism.
[23] M. Borkovec and B. J. Berne, J. Chem. Phys. **82**, 794 (1985).
[24] M. Borkovec, J. E. Straub, and B. J. Berne, J. Chem. Phys. **85**, 146 (1986).
[25] M. Borkovec and B. J. Berne, J. Chem. Phys. **86**, 2444 (1987).
[26] W. L. Hase, in *Dynamics of Molecular Collisions, Part B*, edited by W. H. Miller (Plenum, New York, 1976).
[27] R. F. Grote and J. T. Hynes, J. Chem. Phys. **73**, 2715 (1980).
[28] B. Carmeli and A. Nitzan, Chem. Phys. Lett. **106**, 329 (1984).
[29] J. E. Straub and B. J. Berne, J. Chem. Phys. **85**, 2999 (1986).
[30] E. Pollak, J. Chem. Phys. **85**, 865 (1986).
[31] J. A. Montgomery, Jr., S. L. Holmgren, and D. Chandler, J. Chem. Phys. **73**, 3866 (1980).
[32] J. E. Straub, M. Borkovec, and B. J. Berne, J. Chem. Phys. **83**, 3172 (1985); **84**, 1788 (1986), addendum and erratum; **86**, 1079 (1986). Recently, progress has been made in addressing this problem; see P. Talkner and H. Braun, J. Chem. Phys. **88**, 7537 (1988).
[33] J. E. Straub, M. Borkovec, and B. J. Berne, J. Chem. Phys. **86**, 4296 (1987).
[34] D. J. Evans and G. P. Morriss, Comput. Phys. Rep. **1**, 297 (1984).
[35] APMATH64 Manual, Floating Point Systems, 1983.
[36] D. A. McQuarrie, *Statistical Mechanics* (Harper and Row, New York, 1976).
[37] D. Chandler, *Introduction to Modern Statistical Mechanics* (Oxford University, New York, 1987).
[38] R. Zwanzig, in *Boulder Lectures in Theoretical Physics* (Wiley–Interscience, New York, 1961).
[39] B. J. Berne and R. Pecora, *Dynamic Light Scattering* (Wiley–Interscience, New York, 1976).
[40] R. Zwanzig, Annu. Rev. Phys. Chem. **16**, 67 (1965).
[41] B. J. Berne and G. D. Harp, Adv. Chem. Phys. **17**, 63 (1970); G. D. Harp and B. J. Berne, Phys. Rev. A **2**, 975 (1970).
[42] The exact value of this constant is $a_3 = [\dot{\zeta}(0)/\zeta(0) - \sqrt{\pi/4\alpha}(1 + 3a_1/4\alpha^2) - \sqrt{\pi/\beta}\,(3a_2/8\beta^2)]\sqrt{\gamma/\pi}(16\gamma^3/15)$.
[43] D. Fincham and D. M. Heyes, Chem. Phys. **78**, 425 (1983).
[44] D. Levesque and L. Verlet, Phys. Rev. A **2**, 2514 (1970).

[45]D. Chandler, J. Chem. Phys. **68**, 2959 (1978).
[46]P. Pechukas, in *Dynamics of Molecular Collisions, Part B*, edited by W. H. Miller (Plenum, New York, 1976).
[47]B. J. Berne, in *Multiple Time Scales*, edited by J. U. Brackbill and B. I. Cohen (Academic, New York, 1985).
[48]J. E. Straub and B. J. Berne, J. Chem. Phys. **83**, 1138 (1985); J. E. Straub, D. A. Hsu, and B. J. Berne, J. Phys. Chem. **89**, 5188 (1985).
[49]B. J. Berne, N. DeLeon, and R. O. Rosenberg, J. Phys. Chem. **86**, 2166 (1982).
[50]N. Metropolis, A. W. Rosenbluth, M. N. Rosenbluth, A. H. Teller, and E. Teller, J. Chem. Phys. **21**, 1087 (1953).
[51]W. C. Swope, H. C. Andersen, P. H. Berens, and K. R. Wilson, J. Chem. Phys. **72**, 4350 (1980).
[52]M. Borkovec and B. J. Berne, J. Phys. Chem. **89**, 3994 (1985).
[53]J. O. Hirschfelder, C. F. Curtiss, and R. B. Bird, *Molecular Theory of Gases and Liquids* (Wiley, New York, 1954).
[54]J. Troe, J. Chem. Phys. **66**, 4745 (1977).
[55]*CRC Handbook of Tables for Mathematics*, edited by S. M. Selby (Chemical Rubber, Cleveland, OH, 1970).
[56]A. P. Penner and W. Forst, J. Chem. Phys. **67**, 5296 (1977).
[57]R. Zwanzig, J. Chem. Phys. **86**, 5801 (1987).
[58]R. Zwanzig, J. Stat. Phys. **9**, 215 (1973).
[59]J. P. Bergsma, J. R. Reimers, K. R. Wilson, and J. T. Hynes, J. Chem. Phys. **85**, 5625 (1986).
[60]J. P. Bergsma, B. J. Gertner, K. R. Wilson, and J. T. Hynes, J. Chem. Phys. **86**, 1356 (1987).
[61]A. G. Zawadzki and J. T. Hynes (preprint).
[62]R. A. Kuharski, D. Chandler, J. A. Montgomery, Jr., F. Rabii, and S. J. Singer, J. Phys. Chem. **92**, 3261 (1988).
[63]S. P. Velsko, D. H. Waldeck, and G. R. Fleming, J. Chem. Phys. **78**, 249 (1983).
[64]J. Hicks, M. Vandersall, Z. Babarogic, and K. Eisenthal, Chem. Phys. Lett. **116**, 18 (1985).
[65]H. W. Schranz and J. Troe, J. Phys. Chem. **90**, 6168 (1986).
[66]R. O. Rosenberg, B. J. Berne, and D. Chandler, Chem. Phys. Lett. **75**, 162 (1980).
[67]More accurate analysis is possible. See, for example, K. S. Schweizer and D. Chandler, J. Chem. Phys. **76**, 2296 (1982).